AGU PUBLICATIONS

Geophysical Research Letters

RESEARCH LETTER
10.1002/2017GL076472

Key Points:
- Meridional and seasonal control of radiative forcing using sulfate aerosols is possible—with a limited number of degrees of freedom
- If direct H_2SO_4 injection creates new accumulation mode particles, it enables finer temporal and spatial control of radiative forcing
- There is a sharp trade-off between temporal and spatial control and the amount of sulfur needed per unit of global mean radiative forcing

Supporting Information:
- Supporting Information S1

Correspondence to:
Z. Dai,
zdai@g.harvard.edu

Citation:
Dai, Z., Weisenstein, D. K., & Keith, D. W. (2018). Tailoring meridional and seasonal radiative forcing by sulfate aerosol solar geoengineering. *Geophysical Research Letters, 45*. https://doi.org/10.1002/2017GL076472

Received 30 JUN 2017
Accepted 5 JAN 2018
Accepted article online 8 JAN 2018

©2018. American Geophysical Union. All Rights Reserved.

Tailoring Meridional and Seasonal Radiative Forcing by Sulfate Aerosol Solar Geoengineering

Z. Dai[1], D. K. Weisenstein[1], and D. W. Keith[1,2]

[1]John A. Paulson School of Engineering and Applied Sciences, Harvard University, Cambridge, MA, USA, [2]John F. Kennedy School of Government, Harvard University, Cambridge, MA, USA

Abstract We study the possibility of designing solar radiation management schemes to achieve a desired meridional radiative forcing (RF) profile using a two-dimensional chemistry-transport-aerosol model. Varying SO_2 or H_2SO_4 injection latitude, altitude, and season, we compute RF response functions for a broad range of possible injection schemes, finding that linear combinations of these injection cases can roughly achieve RF profiles that have been proposed to accomplish various climate objectives. Globally averaged RF normalized by the sulfur injection rate (the radiative efficacy) is largest for injections at high altitudes, near the equator, and using emission of H_2SO_4 vapor into an aircraft wake to produce accumulation-mode particles. There is a trade-off between radiative efficacy and control as temporal and spatial control is best achieved with injections at lower altitudes and higher latitudes. These results may inform studies using more realistic models that couple aerosol microphysics, chemistry, and stratospheric dynamics.

1. Introduction

Climate modification by solar geoengineering, or solar radiation management (SRM), is the large-scale intentional manipulation of radiative forcing (RF) to partially and temporarily reduce anthropogenic climate change (Keith, 2000; National Research Council, 2015). A diverse set of studies have explored climate response to variations in meridional or seasonal patterns of SRM RF. Deliberate tailoring of the RF pattern could improve the ability of SRM to achieve specific climate objectives and might allow the reduction of risks or side effects (Keith & MacMartin, 2015; Kravitz et al., 2016). Using a two-dimensional (2-D) chemistry-transport model (CTM) with an aerosol module, we inject SO_2 or accumulation-mode particles at different latitudes, altitudes, and seasons, and then explore the ability to achieve a specific meridional RF profile ("controllability") with linear combinations of these basic scenarios to provide guidance for further experiments with 3-D high-resolution dynamical models.

Many studies on the controllability of SRM schemes have focused on modeling with theoretical top-of-atmosphere RF adjustments. Using meridional and seasonal alterations of top-of-atmosphere RF, MacMartin et al. (2012) showed that regional variations in residual climate change could be reduced, and Kravitz et al. (2016) showed that climate uncertainties could be mitigated through dynamic adjustment of SRM schemes with feedback control. Other studies addressed polar regions, finding, for example, that high-latitude RF could be effective in preserving the Greenland ice sheet (Caldeira & Wood, 2008). Modeling of polar RF reduction showed enhanced cooling at high latitude compared with effects at lower latitude (MacCracken et al., 2013). Regional dimming experiments near the poles revealed that appropriately designed regional solar radiation reduction was needed to preserve arctic sea ice and control northward heat transport (MacMartin et al., 2012; Tilmes et al., 2014).

Most research on specific SRM implementations has focused on increasing the stratospheric sulfate aerosol burden, in part because it is (arguably) the only SRM method with a strong natural analog that can produce relatively uniform global RF of several Wm^{-2} using existing technologies (National Research Council, 2015). A few studies have varied SO_2 injections or sulfate loading choosing specific meridional or seasonal variations (Ban-Weiss & Caldeira, 2010; Haywood et al., 2013; Jackson et al., 2015; Laakso et al., 2017; Niemeier, Schmidt, & Timmreck, 2011; Robock et al., 2008; Tilmes et al., 2017). An early study demonstrated that injection of SO_2 into arctic or equatorial regions resulted in RF changes that extended beyond the regions of injection, causing temperature decrease as well as changes in general circulation pattern and the hydrological cycle (Robock et al., 2008). SO_2 injection above Svalbard with injection amount adjusted annually based on a model predictive control algorithm was shown to preserve the arctic sea ice (Jackson et al., 2015), and SO_2

injection into the stratosphere of either the entire northern or southern hemisphere was shown to cause different impacts on Sahel vegetation (Haywood et al., 2013). Other studies explored global impacts, finding, for example, that specified poleward-peaked aerosol loading was necessary to achieve a climate more similar to the preindustrial one (Ban-Weiss & Caldeira, 2010). Exploration of SO_2 injections into various meridional, zonal, and altitudinal bands found that RF efficacy (RF per unit injection rate) could be increased by decreasing injection rate, limiting the zonal and meridional extents of the injection band, and increasing the injection altitude (Heckendorn et al., 2009; Niemeier & Timmreck, 2015), but these studies did not try to achieve specific control of RF spatial profiles consistent with those used in studies described in the preceding paragraph. Recent WACCM studies did address this issue, albeit with injections at a limited number of locations (Kravitz et al., 2017; MacMartin et al., 2017; Tilmes et al., 2017).

The uncertainty in predicting RF for a given SO_2 injection scenario is highlighted by results from the Geoengineering Model Intercomparison Project (GeoMIP). Kashimura et al. (2017) found substantial intermodel disagreement when they examined results from the GeoMIP G4 simulations, which specify a 5 Mt yr^{-1} SO_2 injection, finding that the globally and temporally averaged forcing varied widely from about -3.6 to -1.6 Wm^{-2} for the six models studied. Large intermodel disagreement in aerosol optical depth also existed due to differences in model transport and different aerosol size distributions (Pitari et al., 2014). It is possible that intramodel disagreement would be reduced using state-of-the-art 3-D high-resolution dynamical models. Such models are, however, computationally expensive, so that it is not practical to simulate the wide range of injection scenarios relevant to assessing the controllability of RF.

The injection of H_2SO_4 vapor into an aircraft wake was proposed by Pierce et al. (2010) to avoid inefficiently large particles produced by SO_2 injection. Pierce et al. used a plume model to account for the rapid nucleation and coagulation of aerosol particles in an expanding aircraft plume, finding that this method could keep the global aerosol size distribution closer to optimal, reducing the flux of sulfur required for a given RF and producing a more linear response of RF to injection flux. English et al. (2012) modeled injection of H_2SO_4 evenly mixed over a GCM grid box and found no benefit over SO_2 injection, a result that does not contradict Pierce et al. (2010) because the production of new appropriately sized accumulation-mode particles depends on the rapid formation of new aerosols in the high-concentration conditions of an expanding plume. Benduhn et al. (2016) modeled possible stratospheric aircraft injection conditions and confirmed that conditions used by Pierce et al. (2010) could produce a radiatively effective aerosol size distribution. Yet no studies have tested the Pierce et al. H_2SO_4 scheme in a GCM. For convenience, we will hereafter refer to injection of accumulation-mode particles that might be produced by injecting H_2SO_4 into an aircraft wake simply as "accumulation mode sulfate (AM-H_2SO_4)" injection.

The controllability of SRM RF using injections of either SO_2 or AM-H_2SO_4 is therefore a vital but inadequately understood link between studies of the climate's response to specified changes in RF and understanding of stratospheric aerosol evolution based on observations and models. Despite the importance of this link, there are no systematic parametric studies of the controllability of RF using sulfate aerosol including in the recent Whole Atmosphere Community Climate Model (WACCM) study (Tilmes et al., 2017). We suspect that this is, in part, because GCMs with comprehensive treatments of aerosols and chemistry are computationally expensive.

We choose to use a 2-D CTM with treatment of sulfate chemistry and aerosol microphysics. Its computational efficiency allows us to systematically explore the injection parameter space, mapping the model response function in latitudinal, altitudinal, and seasonal dimensions. Our intent is to (a) provide a first systematic estimate of the controllability of RF through SO_2 injections, (b) explore AM-H_2SO_4 injection to avoid the approximate 30 day chemical conversion time of SO_2 into H_2SO_4 to achieve finer temporal and spatial control in RF management, and (c) provide guidance for future modeling efforts using 3-D high-resolution dynamical models. Our goal is not to prescribe the "right" answer but to provide guidance to future 3-D numerical experiments.

The range of desirable RF objectives could include achieving globally uniform RF, balancing hemispherical RF to minimize movement of the Intertropical Convergence Zone (ITCZ) and adjust the precipitation centroid, creating more RF reductions around the polar or tropical regions, and creating peak RF during polar summers to maximize the ice-albedo response and preserve sea ice with minimal total RF (Kravitz et al., 2016). Our goal

is not to address the appropriate goal of RF manipulation, but rather to understand the feasibility and limits to RF control.

2. Methods

We use the Atmospheric and Environmental Research (AER) 2-D CTM (Weisenstein et al., 1997, 2004, 2007) simplified to include only chemistries that contribute to sulfate formation, employing O_3 and OH concentrations from previous model calculations. The model uses a sectional representation of the sulfate particle size distribution, with 40 logarithmically-spaced bins from 0.4 nm to 3.2 μm. Microphysical processes including homogeneous nucleation, coagulation, and condensation/evaporation are included in the model, as well as sedimentation and wet deposition. The model has a global domain with 19 latitudinal and 51 altitudinal bins ranging from pole to pole and from the surface to 60 km, with resolution of ~9.5° latitude and ~1.2 km in the vertical. The transport and temperature fields (Fleming et al., 1999) are prescribed based on a climatology from 1978 to 2004 and employ a monthly varying temperature distribution to account for differences from the zonal and monthly means.

We simulate continuous and spatially homogeneous injections of SO_2 or AM-H_2SO_4 in each of the 19 latitudinal bins and 4 vertical layers (10–14 km, 14–17.5 km, 17.5–21 km, and 21–24 km). Only bins completely above the tropopause were chosen (62 total injection cases modeled). The injection flux varied with latitude to achieve a constant flux per unit surface area equivalent to 1 Mt-S $yr^{-1}/4\pi R_{earth}^2$, chosen so that coagulation rates would not depend strongly on latitude. Injections into single latitudinal bands were less than 0.1 Mt-S yr^{-1} in all cases to study the response at the limit of reduced nonlinearity. We then explored linearity with a set of simulation at the highest and lowest altitudes with higher injection rates (1, 2.5, 5, and 10 Mt-S yr^{-1}) at the equator, 66°N and 66°S. The AM-H_2SO_4 injection methodology follows that in Pierce et al. (2010). Sulfur was injected as hydrated sulfate particles with a dry mode radius of 0.095 μm and lognormal distribution width $\sigma = 1.5$ (the result of plume processing of H_2SO_4 gas following injection by aircraft). The model was run for about 10 years in each case to closely approximate steady state.

Instantaneous radiative forcing at the top of atmosphere was computed using Mie theory and published refractive index data for 1,400 spectral channels with the method of Charlson et al. (1991). The diurnal solar illumination geometry for each model time step and latitudinal bin are used with monthly zonal observations of surface albedo, all-sky albedo, and cloud fraction (Doelling, 2017) to calculate the hemispherically integrated reflected radiation.

3. Results

3.1. RF Distribution

Figure 1 summarizes the annually averaged RF efficacy for each SO_2 injection altitude. Injections at higher altitudes result in higher steady state RF. This is mainly due to longer stratospheric residence time of aerosols before they reach the troposphere where removal by cloud scavenging and wet deposition become efficient. The distribution of RF is similar for all injection altitudes, with the highest RF values near the injection latitude for injections near the equator (~±15°), whereas the RF peaks shift poleward relative to injection latitude for extratropical injections. The peaks in the tropics are caused by injections into the upward branch of the Brewer-Dobson circulation and by weak meridional transport caused by the tropical pipe isolation (Plumb, 1996). The poleward shift of RF peaks for midlatitude injection results from poleward Brewer-Dobson transport combined with delay between SO_2 injection and aerosol formation. This shift is complicated for injection at higher latitudes because of low solar insolation closer to the pole. RF efficacies for injections in the southern hemisphere are lower than those in the northern hemisphere due to a stronger polar vortex that enhances downwelling deposition. Injecting AM-H_2SO_4 results in similar RF distribution patterns (see Figure S1 in the supporting information). However, higher RF values are obtained with the same sulfur injection rate due to the smaller aerosol size distribution and slower sedimentation speed of aerosols produced from AM-H_2SO_4 injection. In addition, RF peaks occur much closer to their latitudes of injection because there is no delay in forming aerosol and show deviations mostly because of the latitudinally varying solar insolation. These differences are consistent with the results in Pierce et al. (2010) and English et al. (2012).

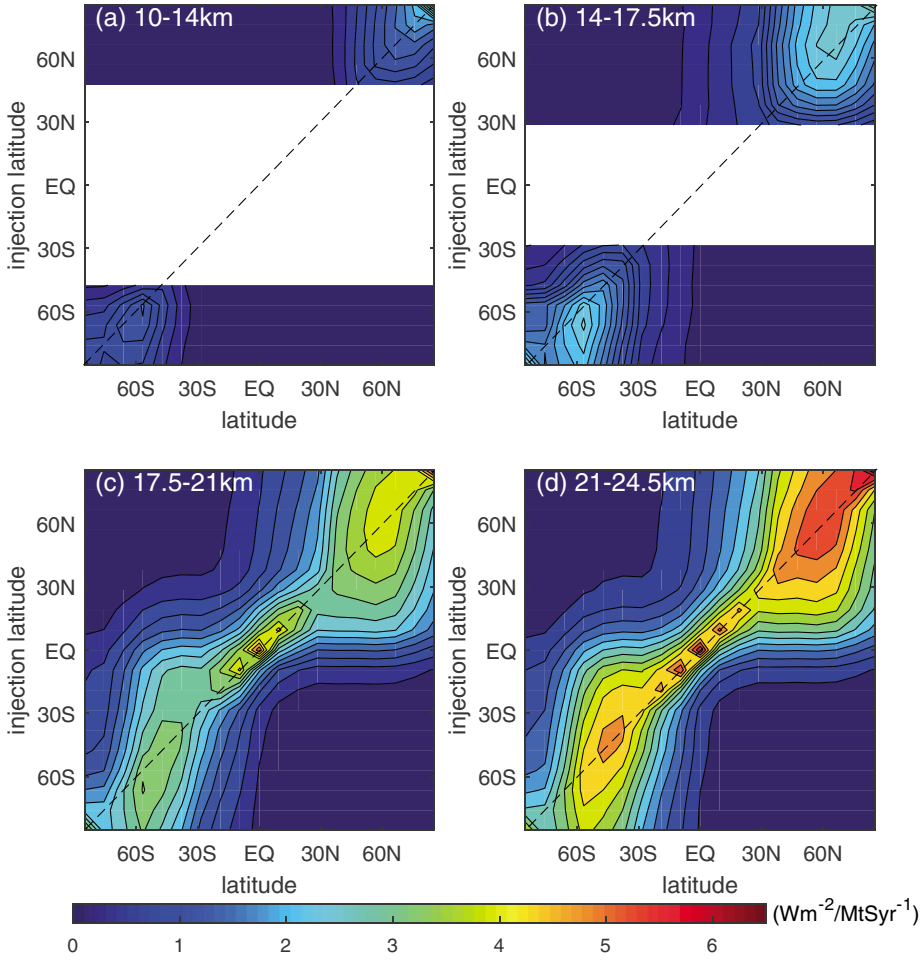

Figure 1. Annually averaged RF efficacies for SO_2 injections at various latitudes as a function of latitude. For every injection latitude on the ordinate, the RF efficacies at corresponding latitudes on the abscissa are represented on the contour plot. Text on each plot represents the injection height. RF values were normalized by injection rates. The dashed black lines on each subplot are added to guide the eye in locating RF peak latitude relative to SO_2 injection latitude. (a and b) Latitudinal bands below the tropopause where no modeling of injection was performed are shown in white.

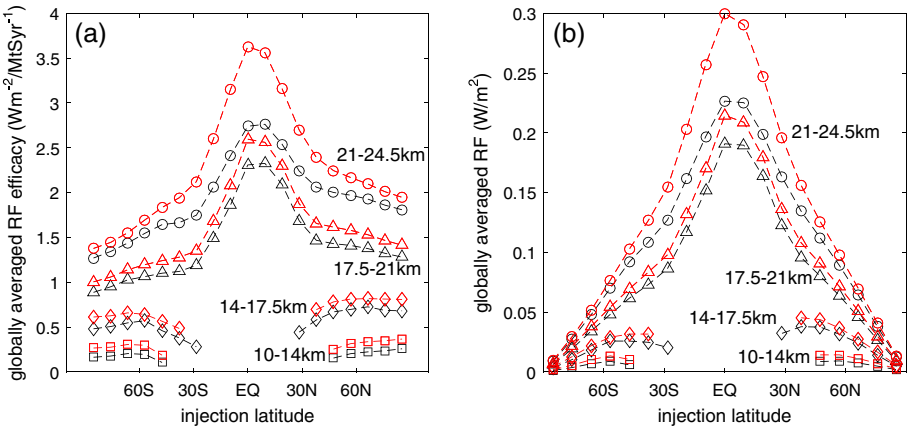

Figure 2. Globally averaged (a) RF efficacies and (b) RF resulting from SO_2 (black) and AM-H_2SO_4 (red) injections. Text represents altitudinal band of injection. The interpolation lines are broken for injections at 10–14 km and 14–17.5 km because no simulations are performed for these low latitude cases.

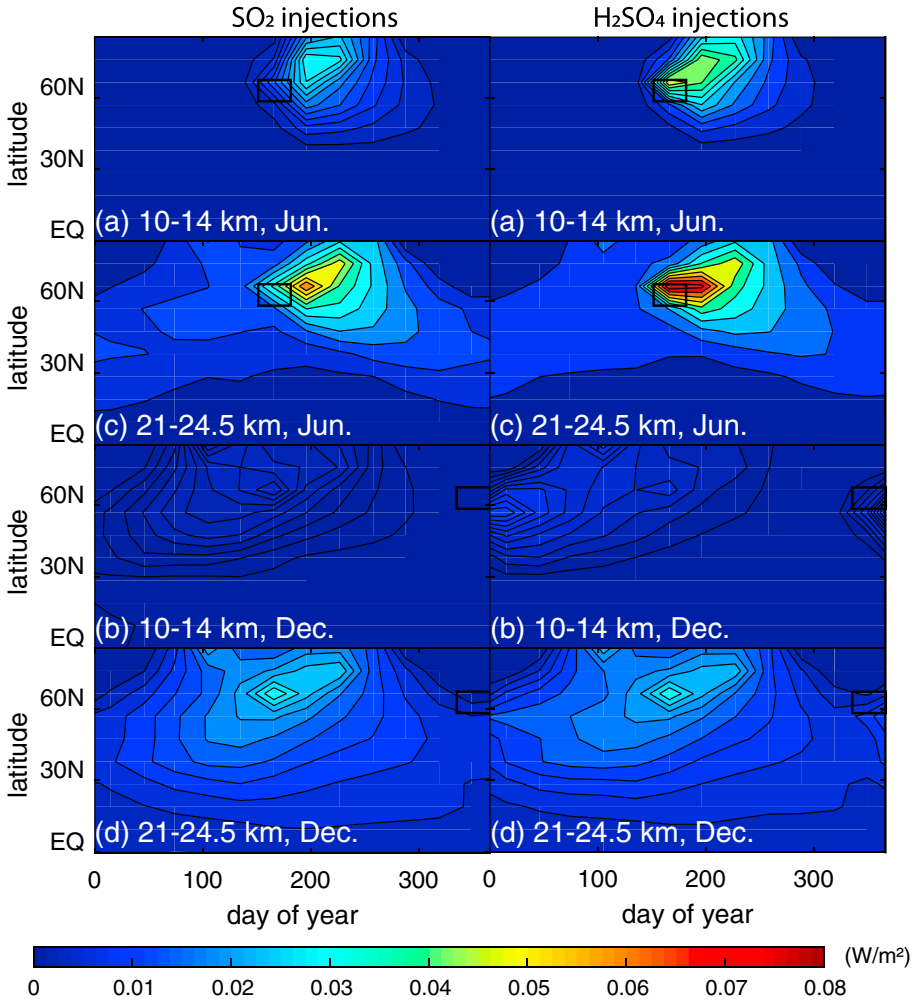

Figure 3. RF distribution from seasonal injections (30 days per year) at the latitudinal band centered at 66.3°N with an injection rate of 0.0028 Mt-S yr^{-1}. Text represents altitudinal band and month of the injection. The black boxes mark the time and latitude of injection.

Globally and annually averaged RF efficacy and corresponding calculated RF are shown in Figure 2. Injections at higher altitudes and tropical latitudes produce the highest RF efficacy. AM-H_2SO_4 injections result in greater RF efficacy than SO_2 injections. Microphysical evolution influenced by aerosol injection strategy and injection location affects RF efficacies. Sulfate aerosols that are 0.3 μm in radius scatter more effectively than ones in the nucleation mode or larger than 0.5 μm (Dykema et al., 2016). Due to the inefficient meridional transport, particles are more confined in the tropical region, giving them time to grow by coagulation and condensation to sizes that scatter light more efficiently for SO_2 injections. Injection of SO_2 is more likely to produce both particles too small (by nucleation) and too large (by coagulation and condensation onto background particles) for efficient scattering, while injection of AM-H_2SO_4, which we model as injection of particles with mode radius 0.095 μm, produces more particles near 0.3 μm (see Pierce et al., 2010, Figure 3).

It should be emphasized that the RF efficacies in this section were derived from small RF values (Figure 2b) as we are interested in first-order responses at small injection rates. These values would decrease significantly at high injections rates. For example, equatorial 5 Mt-S yr^{-1} SO_2 injection at 21–24.5 km results in 0.72 Wm^{-2}/Mt-S yr^{-1}, roughly 20% of the radiative efficacy shown in Figure 2a. Such efficacies are comparable to recent WACCM results (Kravitz et al., 2017), and within the range of GCM results in literature (Pitari et al., 2014). Section 3.3 includes more discussion of expected nonlinearity.

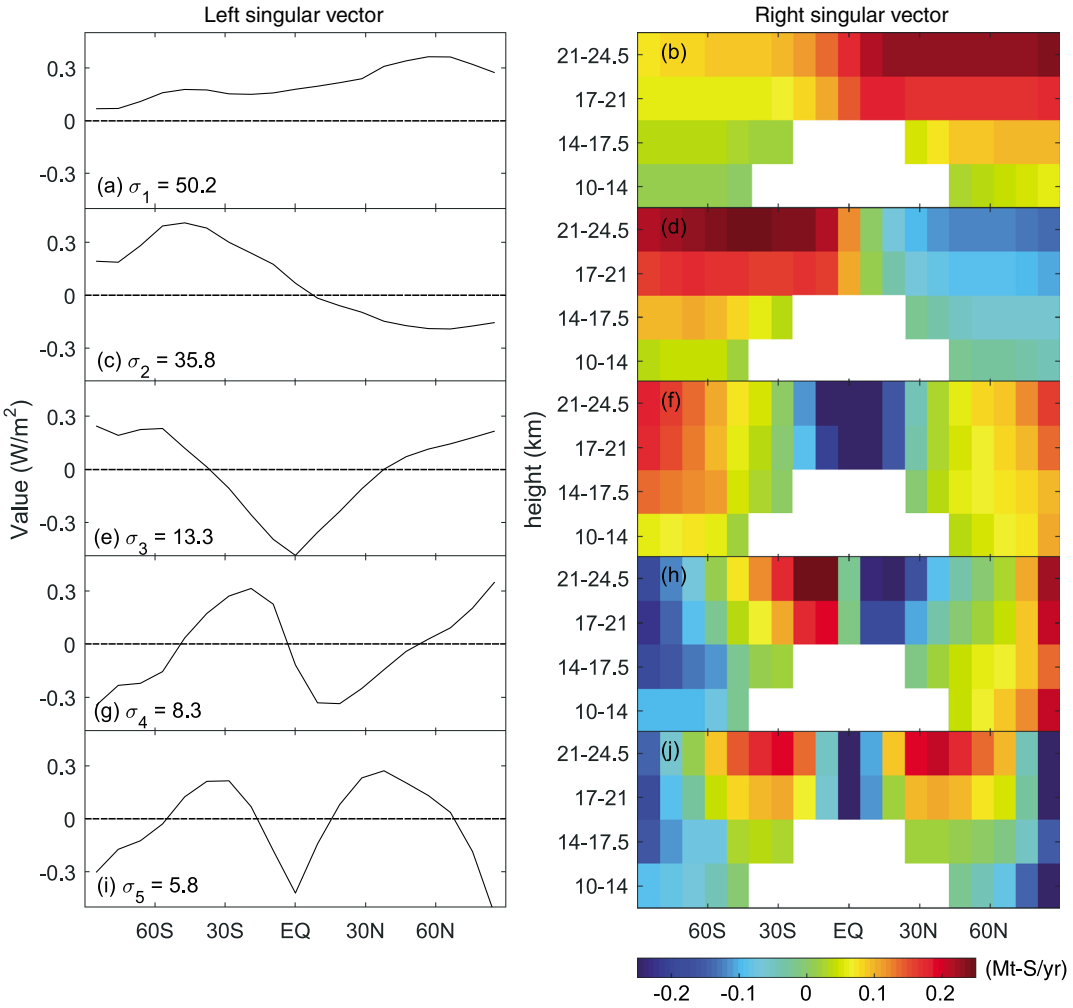

Figure 4. (a–i) Results from singular value decomposition of the RF efficacy matrix showing the first five singular vectors for results from SO_2 injections. Figures 4a, 4c, 4e, 4g, and 4i are the corresponding singular values. The *n*th singular value corresponds to n − 1 latitudinal nodes on the *n*th left singular vector.

3.2. Results From Seasonal Injections

We explore temporal control using a few idealized seasonal injection experiments. One motivating scenario is the possibility of concentrating the SRM perturbation during polar summer to preserve the arctic sea ice while minimizing the global perturbation (MacCracken et al., 2013; MacMartin et al., 2012).

Figure 3 illustrates results from injection scenarios at 66.3°N and two different altitudes for 1 month per year, in June or December. Higher injection altitude produces higher RF for both SO_2 and AM-H_2SO_4 due to longer aerosol residence time while also allowing the plume more time to spread, resulting in a less spatially and temporally confined distribution. SO_2 injections in winter produce peak RF distributions in spring due to minimal SO_2 oxidation and low solar insolation in the polar winter. In contrast with AM-H_2SO_4 injections, the differences between seasonal and spatial oxidation rates play little role in plume formation. Therefore, RF peaks occur closer to the point of injection both spatially and temporally except when the solar insolation is low (polar winter). Thus, better temporal and spatial control is achieved.

3.3. Fitting of Injections to Achieve Specified RF Profiles

We explore the possibility of generating specified RF profiles with linear combinations of injection cases. We use a least-square fitting process constraining injection rates to be positive. The model results act as an

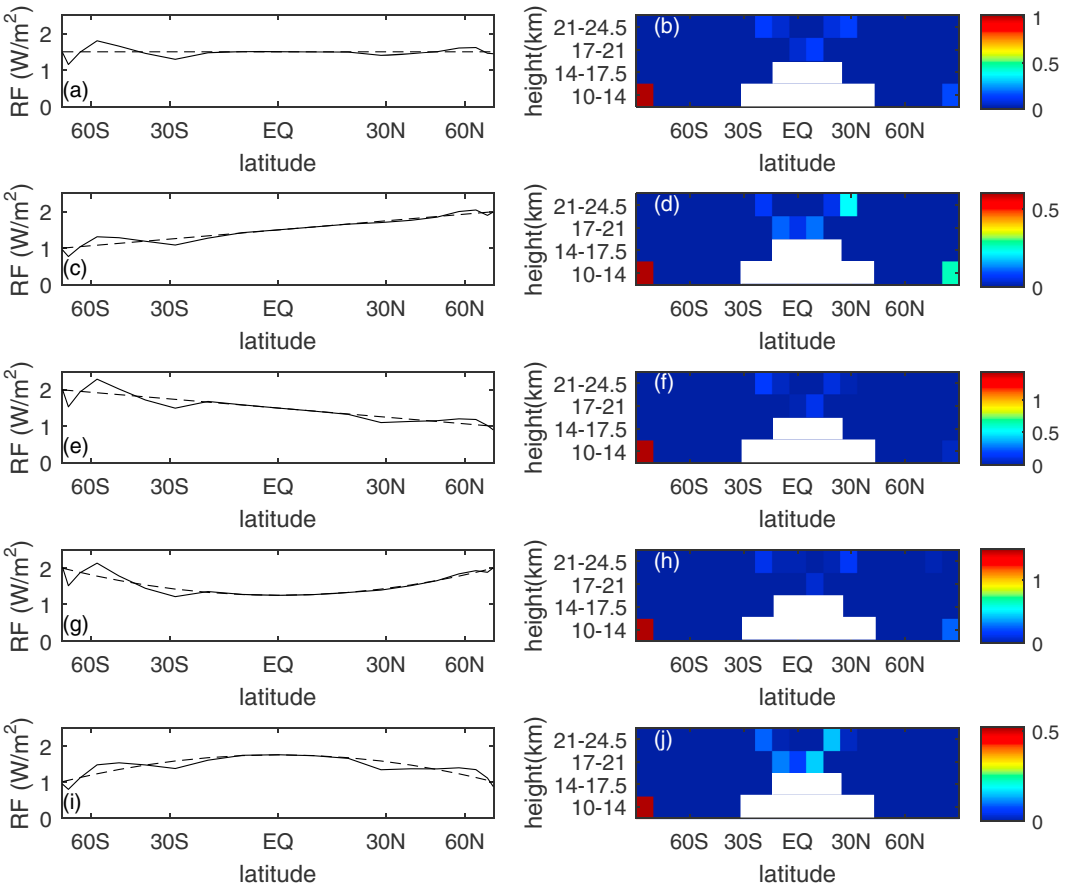

Figure 5. (a–i) Least square fitting results for various possibly desirable global RF profiles that achieve globally averaged RF of 1.5 W/m^2. The dashed lines represent the desired profiles, and the solid lines represent the best fit by scaling RF distribution results from injections with SO_2 at a single latitudinal and altitudinal band. The subplots in the second column (Figures 5b, 5d, 5f, 5h, and 5j) represent injection rates (in Mt-S yr^{-1}) for injections at a latitudinal and altitudinal band to achieve the best fit RF distribution. Bands where no modeling was performed are represented by white squares. Total injection rates to achieve the profiles in Figures 5a, 5c, 5e, 5g, and 5i are 1.51, 1.37, 1.65, 1.93, and 1.08 Mt-S yr^{-1}.

operator that maps from linear combination coefficients to RF profiles. After diagonalization through singular value decomposition (SVD), this operator can be expressed as

$$O = \sum_j |j, U\rangle \sigma_j \langle j, V| \tag{1}$$

where O is a matrix whose column vectors are annually averaged RF efficacies at the 19 latitudinal bands used in the model. It maps from the "injection rate space" (V) to the "zonally averaged RF value space" (U). (Note that left singular vectors were not weighted by zonal areas, as we did not want to discount the importance of achieving polar RF targets.) $\langle j, V|$ and $|j, U\rangle$ are singular vectors in the respective spaces, and σ_j is the corresponding singular value. $|j, U\rangle\langle j, V|$ then represents a rank-one approximation of O, whose weight scales with σ_j. $|j, U\rangle$ and $\frac{1}{\sigma_j}|j, V\rangle$ are the associated RF pattern and the injection rates needed from individual cases to achieve this pattern. Since $\langle j, V|$ and $|j, U\rangle$ are unit vectors, large σ_j represents high root-mean-square (RMS) efficacy (RMS RF/RMS injection rates) in achieving $|j, U\rangle$. The SVD results for SO_2 injection are shown in Figure 4. The AM-H_2SO_4 injection cases show similar patterns (see Figure S2). The first singular vector $|1, U\rangle$ (Figure 4a) shows an upward trend to the north, consistent with our discussion of the north/south comparison in section 3.1. The second singular value is relatively large, signifying relative ease of generating hemispherical contrasts, while higher singular values are substantially smaller, signifying the difficulty of generating higher order variations such as polar peak and equatorial minima or the converse.

We tested linearity by comparing direct calculations with predicted distributions assuming linear additivity of RF (see Figure S3). The RF response to both SO_2 and AM-H_2SO_4 injection is more linear for injections at high latitude and low altitude due to the shorter sulfur lifetime here compared to tropical and high altitude injections, which minimizes coagulation into large particles that have lower radiative efficacy and faster sedimentation rate. AM-H_2SO_4 injection results in better linearity in general. This effect is especially apparent comparing the equatorial high-altitude injection cases (Figure S3b). The low RF efficacies for injections below the tropopause (Figure S3a) also highlight the drawbacks of tropospheric injection schemes that might achieve precise spatial control (Bernstein et al., 2013). The RFs from SO_2 injections at several different locations are close to the linear combination of the individual RFs (Figures S3c and S3d).

Our study shows that injection schemes can be linearly combined to achieve a specific RF objective especially for small magnitude injections outside of the equatorial region consistent with results from MacMartin et al. (2017). This complements previous studies that assessed tuning of prescribed RF profiles to achieve specific climate objectives (Kravitz et al., 2016; Kravitz et al., 2017; MacMartin et al., 2012), suggesting that RF adjustments required in such tuning can indeed be achieved with sulfur injections.

Figure 5 shows results from least-square fitting to desirable profiles commonly mentioned in literature using SO_2 injections (Ban-Weiss & Caldeira, 2010; Kravitz et al., 2016; Kravitz et al., 2017; MacMartin et al., 2012). We achieved reasonable fits to target profiles. Fits using AM-H_2SO_4 injection show similar patterns (see Figure S4). These results are consistent with the SVD analysis, as prominent features from the first and second singular vectors can be seen in all fitting results. Due to low solar insolation in polar regions, large injection rates are required to achieve target RF at the poles. If latitudinal-dependent RF (including polar RF) targets are not essential, errors in the least-square fitting can be weighted by area at each latitudinal bin. Results with this weighting are shown in Figures S5 and S6.

These results are first-order approximations without correction for deviations from linearity. However, since injection rates required are generally low ($<$0.2 Mt-S yr^{-1}) except at the poles, we expect small deviations from the profiles except in polar regions. They provide strong evidence regarding the relative difficulty of achieving various profiles and a starting point for studies using more computationally expensive models.

4. Discussion and Conclusions

The challenge of adjusting SO_2 injection to achieve some climate objective is being tackled by a group using the WACCM high-resolution GCM with a modal aerosol scheme combined with dynamic adjustment of SO_2 injection to demonstrate that feedback can improve control of surface temperature (Kravitz et al., 2017). This result is a major step forward but would be computational challenging for broad parametric explorations such as in this paper.

We suspect that it may be more effective to separate feedback control of RF and climate because they operate on very different timescales. Control of SRM might be approached by adjusting aerosol injection using observations and feedback to "close the loop" and produce an actual aerosol RF distribution that is close to some target (MacMartin et al., 2014). Rather than using surface temperature as a feedback objective as in the WACCM studies, a target RF distribution could be the feedback objective, with that RF target then adjusted much more slowly based on climate response or other factors.

Here we take a complementary approach to systematically explore the RF response to injection of both SO_2 and AM-H_2SO_4 as a function of latitude, altitude, and season. Unlike the WACCM effort, we use a sectional aerosol scheme for accurate simulation of the evolution of aerosol size distributions. We also explore the use of AM-H_2SO_4 injection to improve the control of particle size. Our 2-D CTM cannot capture dynamical feedback to radiative forcing or zonal variability. However, calibration results suggest that the AER 2-D model provides accurate representation of the response to volcanic injections. Therefore, it is appropriate for a parametric exploration of injection schemes.

Our results demonstrate a clear trade-off between spatial control and RF efficacy. As injection altitudes move from stratosphere to troposphere, spatial control at small scales may be possible but at the cost of extremely low efficacy (Bernstein et al., 2013). This trade-off has important consequences for human health and the environment, as sulfate aerosols in the boundary layer pose acute health risks and acidic precipitation causes environmental harm. In considering the consequences of low-altitude injections, we note that in 2010,

emission of 50 Mt-S yr^{-1} was likely responsible for more than a million premature deaths per year (Cohen et al., 2017; Crippa et al., 2016).

This study is among the first to show the potential of achieving desirable RF profiles including an equatorial minimum and linear meridional gradients of either sign. These results are particularly relevant as an equatorial minimum is useful in offsetting the tendency to overcool the equator, which is a common feature of the response to uniform RF (Govindasamy & Caldeira, 2000; Irvine et al., 2016), and the linear gradient is useful in balancing hemispheric forcing to maintain the location of the ITCZ (Kravitz et al., 2016). Our optimization failed to produce a strong equatorial maximum in RF, but this scenario has less practical relevance. We find that linear combinations of injection cases at different latitudes provide a good estimate of the imperfectly linear RF response. Results from AM-H_2SO_4 injections show better linearity when scaling up injection rates than those from SO_2 injections. These results provide a clear basis for experiments with 3-D GCMs and more realistic injection schemes to quantify the possibility of achieving specific RF profiles using feedback control while minimizing environmental side effects of sulfur injection.

Acknowledgments
Funding for this study was provided by a grant from the Fund for Innovative Climate and Energy Research (FICER). We would like to thank Sebastian Eastham and Douglas MacMartin for insightful suggestions on the study design. We would also like to thank John Dykema for providing us the radiative transfer code to calculate AOD and RF. Data generated in the preparation of this work are publicly available on Harvard Dataverse (https://dataverse.harvard.edu/dataverse/zdaiGRL2017, doi:10.7910/DVN/E5MWKU). The authors have no competing financial interest.

References

Ban-Weiss, G. A., & Caldeira, K. (2010). Geoengineering as an optimization problem. *Environmental Research Letters*, *5*(3), 34009. https://doi.org/10.1088/1748-9326/5/3/034009

Benduhn, F., Schallock, J., & Lawrence, M. G. (2016). Early growth dynamical implications for the steerability of stratospheric solar radiation management via sulfur aerosol particles. *Geophysical Research Letters*, *43*, 9956–9963. https://doi.org/10.1002/2016GL070701

Bernstein, D. N., Neelin, J. D., Li, Q. B., & Chen, D. (2013). Could aerosol emissions be used for regional heat wave mitigation? *Atmospheric Chemistry and Physics*, *13*(13), 6373–6390. https://doi.org/10.5194/acp-13-6373-2013

Caldeira, K., & Wood, L. (2008). Global and Arctic climate engineering: Numerical model studies. *Philosophical Transactions of the Royal Society A - Mathematical Physical and Engineering Sciences*, *366*(1882), 4039–4056. https://doi.org/10.1098/rsta.2008.0132

Charlson, R. J., Langner, J., Rodhe, H., Leovy, C. B., & Warren, S. G. (1991). Perturbation of the northern hemisphere radiative balance by backscattering from anthropogenic sulfate aerosols*. *Tellus A*, *43AB*, 152–163. https://doi.org/10.3402/tellusa.v43i4.11944

Cohen, A. J., Brauer, M., Burnett, R., Anderson, H. R., Frostad, J., Estep, K., … Forouzanfar, M. H. (2017). Estimates and 25-year trends of the global burden of disease attributable to ambient air pollution: An analysis of data from the Global Burden of Diseases Study 2015. *Lancet*, *389*(10082), 1907–1918. https://doi.org/10.1016/S0140-6736(17)30505-6

Crippa, M., Janssens-Maenhout, G., Dentener, F., Guizzardi, D., Sindelarova, K., Muntean, M., … Granier, C. (2016). Forty years of improvements in European air quality: Regional policy-industry interactions with global impacts. *Atmospheric Chemistry and Physics*, *16*(6), 3825–3841. https://doi.org/10.5194/acp-16-3825-2016

Doelling, D. (2017). CERES SYN1DEG-MONTH HDF4 file - Edition 4A [Data set]. NASA Langley Atmospheric Science Data Center DAAC. Retrieved from https://doi.org/10.5067/terra+aqua/ceres/syn1degmonth_l3.004a

Dykema, J. A., Keith, D. W., & Keutsch, F. N. (2016). Improved aerosol radiative properties as a foundation for solar geoengineering risk assessment. *Geophysical Research Letters*, *43*, 7758–7766. https://doi.org/10.1002/2016GL069258

English, J. M., Toon, O. B., & Mills, M. J. (2012). Microphysical simulations of sulfur burdens from stratospheric sulfur geoengineering. *Atmospheric Chemistry and Physics*, *12*(10), 4775–4793. https://doi.org/10.5194/acp-12-4775-2012

Fleming, E. L., Jackman, C. H., Stolarski, R. S., & Considine, D. B. (1999). Simulation of stratospheric tracers using an improved empirically based two-dimensional model transport formulation. *Journal of Geophysical Research*, *104*(D19), 23,911–23,934. https://doi.org/10.1029/1999JD900332

Govindasamy, B., & Caldeira, K. (2000). Geoengineering Earth's radiation balance to mitigate CO_2-induced climate change. *Geophysical Research Letters*, *27*(14), 2141–2144. https://doi.org/10.1029/1999GL006086

Haywood, J. M., Jones, A., Bellouin, N., & Stephenson, D. (2013). Asymmetric forcing from stratospheric aerosols impacts Sahelian rainfall. *Nature Climate Change*, *3*(7), 660–665. https://doi.org/10.1038/nclimate1857

Heckendorn, P., Weisenstein, D., Fueglistaler, S., Luo, B. P., Rozanov, E., Schraner, M., … Peter, T. (2009). The impact of geoengineering aerosols on stratospheric temperature and ozone. *Environmental Research Letters*, *4*(4), 45108. https://doi.org/10.1088/1748-9326/4/4/045108

Irvine, P. J., Kravitz, B., Lawrence, M. G., & Muri, H. (2016). An overview of the Earth system science of solar geoengineering. *Wiley Interdisciplinary Reviews: Climate Change*, *7*(6), 815–833. https://doi.org/10.1002/wcc.423

Jackson, L. S., Crook, J. A., Jarvis, A., Leedal, D., Ridgwell, A., Vaughan, N., & Forster, P. M. (2015). Assessing the controllability of Arctic sea ice extent by sulfate aerosol geoengineering. *Geophysical Research Letters*, *42*, 1223–1231. https://doi.org/10.1002/2014GL062240

Kashimura, H., Abe, M., Watanabe, S., Sekiya, T., Ji, D., Moore, J. C., … Kravitz, B. (2017). Shortwave radiative forcing, rapid adjustment, and feedback to the surface by sulfate geoengineering: Analysis of the Geoengineering Model Intercomparison Project G4 scenario. *Atmospheric Chemistry and Physics*, *17*(5), 3339–3356. https://doi.org/10.5194/acp-17-3339-2017

Keith, D. W. (2000). Geoengineering the climate: History and prospects. *Annual Review of Energy and the Environment*, *25*(1), 245–284. https://doi.org/10.1146/annurev.energy.25.1.245

Keith, D. W., & MacMartin, D. G. (2015). A temporary, moderate and responsive scenario for solar geoengineering. *Nature Climate Change*, *5*(3), 201–206. https://doi.org/10.1038/nclimate2493

Kravitz, B., MacMartin, D. G., Mills, M. J., Richter, J. H., Tilmes, S., Lamarque, J.-F., … Vitt, F. (2017). First simulations of designing stratospheric sulfate aerosol geoengineering to meet multiple simultaneous climate objectives. *Journal of Geophysical Research: Atmospheres*, *122*, 12,616–12,634. https://doi.org/10.1002/2017JD026874

Kravitz, B., Macmartin, D. G., Wang, H., & Rasch, P. J. (2016). Geoengineering as a design problem. *Earth System Dynamics*, *7*(2), 469–497. https://doi.org/10.5194/esd-7-469-2016

Laakso, A., Korhonen, H., Romakkaniemi, S., & Kokkola, H. (2017). Radiative and climate effects of stratospheric sulfur geoengineering using seasonally varying injection areas. *Atmospheric Chemistry and Physics*, *17*(11), 6957–6974. https://doi.org/10.5194/acp-17-6957-2017

MacCracken, M. C., Shin, H.-J., Caldeira, K., & Ban-Weiss, G. A. (2013). Climate response to imposed solar radiation reductions in high latitudes. *Earth System Dynamics*, *4*(2), 301–315. https://doi.org/10.5194/esd-4-301-2013

MacMartin, D. G., Keith, D. W., Kravitz, B., & Caldeira, K. (2012). Management of trade-offs in geoengineering through optimal choice of non-uniform radiative forcing. *Nature Climate Change*, *3*(4), 365–368. https://doi.org/10.1038/nclimate1722

MacMartin, D. G., Kravitz, B., Keith, D. W., & Jarvis, A. (2014). Dynamics of the coupled human-climate system resulting from closed-loop control of solar geoengineering. *Climate Dynamics*, *43*(1-2), 243–258. https://doi.org/10.1007/s00382-013-1822-9

MacMartin, D. G., Kravitz, B., Tilmes, S., Richter, J. H., Mills, M. J., Lamarque, J.-F., … Vitt, F. (2017). The climate response to stratospheric aerosol geoengineering can be tailored using multiple injection locations. *Journal of Geophysical Research: Atmospheres*, *122*, 12,574–12,590. https://doi.org/10.1002/2017JD026868

National Research Council (2015). Climate intervention: Reflecting sunlight to cool Earth.

Niemeier, U., Schmidt, H., & Timmreck, C. (2011). The dependency of geoengineered sulfate aerosol on the emission strategy. *Atmospheric Science Letters*, *12*(2), 189–194. https://doi.org/10.1002/asl.304

Niemeier, U., & Timmreck, C. (2015). What is the limit of climate engineering by stratospheric injection of SO_2? *Atmospheric Chemistry and Physics*, *15*(16), 9129–9141. https://doi.org/10.5194/acp-15-9129-2015

Pierce, J. R., Weisenstein, D. K., Heckendorn, P., Peter, T., & Keith, D. W. (2010). Efficient formation of stratospheric aerosol for climate engineering by emission of condensible vapor from aircraft. *Geophysical Research Letters*, *37*, L18805. https://doi.org/10.1029/2010GL043975

Pitari, G., Aquila, V., Kravitz, B., Robock, A., Watanabe, S., Cionni, I., … Tilmes, S. (2014). Stratospheric ozone response to sulfate geoengineering: Results from the Geoengineering Model Intercomparison Project (GeoMIP). *Journal of Geophysical Research: Atmospheres*, *119*, 2629–2653. https://doi.org/10.1002/2013JD020566

Plumb, R. A. (1996). A "tropical pipe" model of stratospheric transport. *Journal of Geophysical Research*, *101*(D2), 3957–3972. https://doi.org/10.1029/95JD03002

Robock, A., Oman, L., & Stenchikov, G. L. (2008). Regional climate responses to geoengineering with tropical and Arctic SO_2 injections. *Journal of Geophysical Research*, *113*, D16101. https://doi.org/10.1029/2008JD010050

Tilmes, S., Jahn, A., Kay, J. E., Holland, M., & Lamarque, J. (2014). Can regional climate engineering save the summer Arctic sea ice? *Geophysical Research Letters*, *41*, 880–885. https://doi.org/10.1002/2013GL058731

Tilmes, S., Richter, J. H., Mills, M. J., Kravitz, B., MacMartin, D. G., Vitt, F., … Lamarque, J.-F. (2017). Sensitivity of aerosol distribution and climate response to stratospheric SO_2 injection locations. *Journal of Geophysical Research: Atmospheres*, *122*, 12,591–12,615. https://doi.org/10.1002/2017JD026888

Weisenstein, D. K., Eluszkiewicz, J., Ko, M. K. W., Scott, C. J., Jackman, C. H., Fleming, E. L., … Rotman, D. A. (2004). Separating chemistry and transport effects in two-dimensional models. *Journal of Geophysical Research*, *109*, D18310. https://doi.org/10.1029/2004JD004744

Weisenstein, D. K., Penner, J. E., Herzog, M., & Liu, X. (2007). Global 2-D intercomparison of sectional and modal aerosol modules. *Atmospheric Chemistry and Physics*, *7*(9), 2339–2355. https://doi.org/10.5194/acp-7-2339-2007

Weisenstein, D. K., Yue, G. K., Ko, M. K. W., Sze, N.-D., Rodriguez, J. M., & Scott, C. J. (1997). A two-dimensional model of sulfur species and aerosols. *Journal of Geophysical Research*, *102*(D11), 13,019–13,035. https://doi.org/10.1029/97JD00901